Environ Sci Pollut Res (2018) 25:25757–25771
DOI 10.1007/s11356-017-0125-9

ENVIRONMENTAL FUNCTIONS OF BIOCHAR

Biochar composites with nano zerovalent iron and eggshell powder for nitrate removal from aqueous solution with coexisting chloride ions

Munir Ahmad[1] · **Mahtab Ahmad**[1,2] · **Adel R. A. Usman**[1,3] · **Abdullah S. Al-Faraj**[1] · **Adel S. Abduljabbar**[4] · **Mohammad I. Al-Wabel**[1]

Received: 29 December 2016 / Accepted: 5 September 2017 / Published online: 18 September 2017

Abstract Biochar (BC) was produced from date palm tree leaves and its composites were prepared with nano zerovalent iron (nZVI-BC) and hen eggshell powder (EP-BC). The produced BC and its composites were characterized by SEM, XRD, BET, and FTIR for surface structural, mineralogical, and chemical groups and tested for their efficiency for nitrate removal from aqueous solutions in the presence and absence of chloride ions. The incidence of graphene and nano zerovalent iron (Fe^0) in the nZVI-BC composite was confirmed by XRD. The nZVI-BC composite possessed highest surface area (220.92 $m^2\ g^{-1}$), carbon (80.55%), nitrogen (3.78%), and hydrogen (11.09%) contents compared to other materials. Nitrate sorption data was fitted well to the Langmuir (R^2 = 0.93–0.98) and Freundlich (R^2 = 0.90–0.99) isotherms. The sorption kinetics was adequately explained by the pseudo-second-order, power function, and Elovich models. The nZVI-BC composite showed highest Langmuir predicted sorption capacity (148.10 mg g^{-1}) followed by EP-BC composite (72.77 mg g^{-1}). In addition to the high surface area, the higher nitrate removal capacity of nZVI-BC composite could be attributed to the combination of two processes, i.e., chemisorption (outer-sphere complexation) and reduction of nitrate to ammonia or nitrogen by Fe^0. The appearance of Fe-O stretching and N-H bonds in post-sorption FTIR spectra of nZVI-BC composite suggested the occurrence of redox reaction and formation of Fe compound with N, such as ferric nitrate ($Fe(NO_3)_3{\cdot}9H_2O$). Coexistence of chloride ions negatively influenced the nitrate sorption. The decrease in nitrate sorption with increasing chloride ion concentration was observed, which could be due to the competition of free active sites on the sorbents between nitrate and chloride ions. The nZVI-BC composite exhibited higher nitrate removal efficiency compared to other materials even in the presence of highest concentration (100 mg L^{-1}) of coexisting chloride ion.

Keywords Chemisorption · Isotherm sorption · Kinetic sorption · Nano zerovalent iron · Nitrate reduction

Responsible editor: Philippe Garrigues

Electronic supplementary material The online version of this article (https://doi.org/10.1007/s11356-017-0125-9) contains supplementary material, which is available to authorized users.

✉ Mohammad I. Al-Wabel
malwabel@ksu.edu.sa

[1] Soil Sciences Department, College of Food & Agricultural Sciences, King Saud University, P.O. Box 2460, Riyadh 11451, Kingdom of Saudi Arabia

[2] Department of Environmental Sciences, Faculty of Biological Sciences, Quaid-i-Azam University, Islamabad 45320, Pakistan

[3] Department of Soils and Water, Faculty of Agriculture, Assiut University, Assiut 71526, Egypt

[4] Industrial Psychology, College of Education, King Saud University, Riyadh, Saudi Arabia

Introduction

Human intake of nitrate (an inorganic form of nitrogen) through food and water supply has raised twofold of the acceptable daily intake (ADI) recommended by World Health Organization (0–3.7 mg nitrate kg^{-1} of body weight) due to extensive imbalance fertilization intensities (Dobermann and Cassman 2005; ATSDR 2013). No doubt nitrogen is an essential element for life (an integral part of proteins), but excessive nitrogen in the environment is causing severe problems. Nitrogen fertilization, animal manure, and atmospheric nitrogen deposition are the major sources of nitrogen to enter into the food chain through dietary crops and to groundwater

through leaching from surface and subsurface soils (Landon et al. 2000; Xue et al. 2015). Elevated nitrate levels produce eutrophication resulting in toxic algal blooms which have paralytic, diarrheic, and neurotoxic effects on humans, animals, and aquatic life (Flechard et al. 2011; Richardson 1997). According to the WHO, maximum permissible limit of nitrate in drinking water is 50 mg L^{-1} (WHO 2011). Higher levels of nitrate in human can cause hemoglobinemia (blue baby syndrome), cancer (through *N*-nitroso compounds), spontaneous abortions, DNA damage, and increased oxidative stress (Ying and Hofseth 2007; Weyer et al. 2001). Thus, excessive nitrate should be removed from the water and prevented from leaching/seepage from the soil to groundwater. But, due to its higher solubility and lower affinity towards precipitation and adsorption, nitrate removal from water using conventional treatment methods may be inefficient (Islam et al. 2010). Additionally, the presence of coexisting ions, such as chloride, carbonate, sulfate, and phosphate, adversely affect the nitrate sorption due to competition for the active sorption sites. Therefore, there is a dire need to develop new techniques for an efficient nitrate removal from wastewater streams.

Biochar-based materials have come up in recent years as cost-effective and eco-friendly green adsorbents for the remediation of contaminated soil and water. Biochar is a stable, solid, porous carbonaceous material, with large surface area and functional groups, resistant to mineralization and decomposition and produced by pyrolysis of wood, grass, manure, sludge, etc. (Wardle et al. 2008; Beesley et al. 2010; Beck et al. 2011). As the biochar is generally obtained from waste materials, it is considered to be cost-effective and environment-friendly remediation technology. But, due to their heterogeneous composition, biochars possess low to medium adsorption capacities (Loganathan et al. 2013). Furthermore, biochars may be inefficient for anion (such as NO_3) removal from wastewater streams, mainly due to their net negative surface charges. Therefore, attention is now being given to modify biochar's structural and physiochemical properties to improve its adsorption capacity. For instance, incorporation of reducing agents such as zerovalent iron into biochar matrix may enhance its adsorption capacity (Devi and Saroh 2014). Due to lower costs, higher surface area, reductive nature and nanoscale particle size, nano zerovalent iron (nZVI) are highly reactive and can remediate a range of environmental contaminants such as nitroaromatics, hydrocarbons, toxic metal ions, and perchlorates from aqueous media (Chatterjee et al. 2010; Meng et al. 2006; Zhao et al. 2008; Xu et al. 2010; Chang et al. 2011). In spite of higher efficiency and reactivity, practical applicability of nZVI is restricted because of rapid oxidation in air and agglomeration/aggregation in aqueous media due to high surface energy and magnetic interaction (Phenrat et al. 2006; Devi and Saroh 2014). Therefore, using biochar matrix as a support material to composite nZVI can produce a stable nano zerovalent iron with reduced agglomeration and enhanced practical applicability (Wu et al. 2013). Moreover, the presence of nZVI develops a magnetic composite, which can easily be separated from the aqueous solution after loading. Hence, the nZVI-composited biochar may combine the advantages of biochar (sorptive characteristics) and zerovalent iron (reductive characteristics) for efficient removal of potential environmental contaminants. According to our literature review, date palm tree leaf-derived biochar has not been composited with nZVI previously. Moreover, the efficiency of nZVI-composited biochar for nitrate (reducible to nitrite, ammonia, or nitrogen with nZVI) removal has not been investigated yet.

Likewise, the biochar can also be composited with other adsorbents derived from waste materials such as eggshell powder. About 250,000 t of eggshell waste is being produced annually around the globe (Raihana et al. 2008). Calcium carbonate ($CaCO_3$) is the major constituent of eggshell, comprising 85–96% of eggshell composition (Oliveira et al. 2013; Ahmad et al., 2017a). If thermalized at 600–900 °C, the $CaCO_3$ contents in eggshell powder convert to CaO (Buasri et al. 2013). Eggshell ($CaCO_3$) and thermalized eggshell (CaO) powders have been used by many researchers for the immobilization and sorption of a range of environmental pollutants, such as metals ions and inorganic ions (Guru and Dash 2014). Utilization of this waste to produce adsorbents not only reduces surface pollution but also provides a cost-effective technique for contaminants removal. Eggshell powder composited with biochar may combine the advantages of biochar and $CaCO_3$/CaO, which might efficiently be applied for the removal of anions such as nitrate. To our knowledge, biochar composite with eggshell powder has not been reported earlier for adsorption of contaminants in aqueous solution.

Therefore, we propose to utilize biochar as a support material to fabricate nano zerovalent iron-composited biochar with magnetic and reductive properties and higher sorption affinity for nitrate ions. Similarly, we propose to synthesize eggshell waste-composited biochar with improved surface and physiochemical characteristics for efficient nitrate sorption from water compared to pristine eggshell and biochar materials. Additionally, the effect of coexisting chloride ions on the removal of nitrate from aqueous solution was investigated.

Materials and methods

Biochar production

Date palm tree waste (rachis and stems) was collected from the agricultural farms in Riyadh City, Saudi Arabia, washed to remove dust and impurities, and dried in air under the sunshine. The leaves were separated and cut into small pieces (2.5 to 5 cm), ground with a mechanical grinder, and sieved

through 0.6-mm screen. A known amount of processed date palm leaf biomass (BM) was kept in loosely covered crucibles and slowly pyrolyzed at 5 °C min in a tube furnace (Carbolite, type 3216, UK) in the oxygen-limited environment at 600 °C for 3 h. After pyrolysis, crucibles were cooled down in the furnace and kept in a desiccator for 30 min to remove moisture. After recording the weight, the biochar (BC) sample was washed thrice with deionized water to remove soluble ions, ground, and stored in airtight containers.

Synthesis of nano zerovalent iron-composited biochar

Nano zerovalent iron-composited biochar (nZVI-BC) was synthesized by modifying the procedures of Sun et al. (2006) and Yuvakkumar et al. (2011) and combining it with the procedure reported by Yan et al. (2015) and Zhou et al. (2014). Iron sulfate ($FeSO_4{\cdot}7H_2O$) was used as an iron source and sodium borohydride ($NaBH_4$) as a reducing agent. Chitosan was used as a binding agent for cross-linkage. The whole procedure was accomplished in an inert atmosphere to avoid oxidation and to reduce the particle size of Fe (Gupta and Gupta 2005; Kim et al. 2001). Nano zerovalent iron was produced with following reaction shown in Eq. 1 (Uzum et al. 2008):

$$Fe^{2+} + 2BH_4^- + 6H_2O \rightarrow Fe^0 + 2B(OH)_3 + 7H_2\uparrow \quad (1)$$

Specifically, 100 ml of 1 M $FeSO_4{\cdot}7H_2O$ solution was prepared in a mixture of 4:1 (*v*/*v* ratio) ethanol to water and added into a three-neck flask (Fig. S1). Biochar was added to the flask based on 1:1 (*w*/*w* ratio) of BC to elemental iron in the solution (5.6 g BC). The pH of the suspension was adjusted at 5 with H_2SO_4 (5 N). The suspension was vigorously stirred for 2 h with a magnetic stirrer and then purged with N_2 gas for 1 h while stirring. One hundred milliliters of 2 M $NaBH_4$ solution (in DI water) was added dropwise to the flask under vigorous stirring and continuous flow of N_2. The reaction occurred immediately and nano zerovalent iron (Fe^0, nZVI) particles started to precipitate and deposit on biochar matrix. The reaction continued until H_2 gas emission ceased bubbling into a water beaker. After that, 1.12 g chitosan dissolved in 2% acetic acid was added to the flask and stirred for 30 min, under N_2 flow. Then, 100 ml of 1.2% NaOH solution was added slowly to the suspension under gentle stirring. Nitrogen purging was stopped, H_2 outlet and $NaBH_4$ inlet were sealed to avoid O_2 entrance, and suspensions were kept overnight at room temperature undisturbed to facilitate binding between BC and nZVI particles. The precipitated solid material in the bottom of the flask was separated from aqueous solution by decanting the liquid and washed several times with ethanol to get rid of all extra sulfates and iron particles by monitoring its electrical conductivity (EC). While washing, minimum exposure of the solid particles to air was ensured by adding ethanol quickly to the flask after decanting the previous. The middle neck of the flask was then sealed and H_2 outlet was fitted with a coiled condenser whose other end was kept in water beaker to avoid backflow of atmospheric oxygen. The flask was kept in water bath at 100 °C under continuous N_2 supply. Remaining ethanol in the solid material was evaporated with heat and carried to the condenser with N_2 flow. Heating was continued until all the liquid vent out leaving a blackish fine powder of nZVI-BC composite, which was collected and stored in airtight container.

Synthesis of eggshell powder-composited biochar

Waste hen eggshells were collected from a student restaurant at King Saud University, Riyadh, soaked in boiling distilled water, and washed four times to remove impurities. The washed eggshells were dried in an oven at 80 °C for 24 h, powdered with an electric grinder, sieved through 0.6-mm aperture, stored in airtight container, and labeled as EP. Of ground BM, 100 g was taken in a crucible and 10 g of EP was spread on its surface to make a uniform layer on the BM. The crucible was covered tightly and slowly pyrolyzed at 5 °C min in a tube furnace (Carbolite, type 3216, UK) in the oxygen-limited environment at 600 °C for 3 h. After pyrolysis, the crucibles were cooled inside the furnace and then kept in a desiccator for 30 min to remove moisture. After recording the weight, the prepared material was mixed thoroughly to produce eggshell powder-composited biochar (EP-BC). This composite was washed thrice with deionized water, ground, and stored in an airtight container.

Characterization of the synthesized materials

Yield, proximate, and chemical analysis

The percent yield of the produced biochar composites was calculated as:

$$Yield\ (\%) = \frac{Weight\ of\ biomass - Weight\ of\ biochar}{Weight\ of\ biomass} \times 100 \quad (2)$$

Biomass, biochar, and produced composites were subjected to proximate analysis such as moisture, ash contents, and volatile matter, following the standard method of ASTM D1762-84 (ASTM 1989), while resident matter (fixed carbon) was calculated with difference method. Electrical conductivity and pH of the materials were determined in 1:10 (1 g material in 10 ml DI water) suspension. Cation exchange capacity of the composites was measured by ammonium acetate extraction method (Richard 1954). Active carbon fraction was determined following the method described by Blair et al. (1995). Non-labile carbon fraction was calculated by the

difference between active carbon and total carbon analyzed by CHNSO elemental analyzer.

Elemental composition

Elemental composition of pristine materials and produced composites was assessed through CHNSO elemental analyzer (series II, PerkinElmer, USA). Percent carbon (C), hydrogen (H), N, and S were determined through the instrument, while oxygen (O) was calculated using the following equation:

$$\mathrm{O}\ (\%) = 100 - [\mathrm{C}\ (\%) + \mathrm{H}\ (\%) + \mathrm{N}\ (\%) + \mathrm{S}\ (\%) + \mathrm{ash}\ (\%)] \quad (3)$$

Atomic ratios of the elements such as O/C and H/C were also calculated to present the aromaticity and polarity of the materials.

SEM, TGA, FTIR, XRD, and BET analysis

To observe surface morphology and structural changes induced by physiochemical modifications, the composite materials were analyzed using scanning electron microscope (SEM; EFI S50 Inspect, Netherlands). Samples were spread on aluminum stubs coated with adhesive carbon tapes (12 mm; PELCO, UK) and coated with nano-gold particles for 60 s using 108 Auto/SE Sputter Coater (Ted Pella Inc. USA). Images were taken in the range of ×2000–300 magnification at an acceleration voltage of 30 kV under high vacuum. Thermal stability of pristine materials and their derived composites was analyzed using a thermogravimetric analyzer (DTG-60H, Shimadzu, Japan). Weight loss of the materials was recorded with the rise in temperature from 0 to 1100 °C. The composition of structural and functional groups of pristine materials and their derived composite materials was determined using Fourier transform infrared spectroscopy (Bruker Alpha-Eco ATR-FTIR, Bruker Optics Inc.). To analyze various mineralogical phases of the produced materials, X-ray diffractometer (MAXima_X XRD-7000, Shimadzu, Japan) was used with 30 mA Cu Kα radiation at the scan speed of 2° min^{-1} in continuous scan mode. Surface area, total pore volume, and pore diameter were analyzed through Brunauer–Emmett–Teller (BET) method using surface area and porosity analyzer (TriStar II 3020, Micromeritics, USA).

Kinetic sorption experiments

A single solute working solution containing 200 mg L^{-1} of nitrate was prepared in deionized water (18.2 MΩ cm^{-1} resistivity; Milli-Q, Millipore, Germany) along with a blank for each material (without NO_3^- ions) using nitrate standards (Hach Company, USA). A 40-ml single solute solution was taken in a polypropylene conical tube and the above-prepared adsorbents were added at the rate of 1 g L^{-1}. The tubes were shaken horizontally on a mechanical shaker at 150 rpm. Each adsorbent was replicated thrice along with a blank (without adsorbent). Three samples of each material and a blank were withdrawn after 0, 0.16, 0.32, 0.65, 1, 2, 3, 5, 8, 12, and 24 h. The solution was separated from the materials by centrifugation at 3500 rpm for 20 min, filtered through Whatman filter paper, and nitrate ions were determined by the procedure reported by Jagessar and Sooknundun (2011). Briefly, 5 ml of sample from the solution was poured in a crucible and placed in water bath at 80 °C. After complete dryness, the crucible was cooled and 2 ml of phenoldisulfonic acid was added to wash all the contents bonded to the walls. The crucible was shaken gently to make sure that all the contents are in the solution. After 30 min, 10 ml of concentrated ammonium hydroxide was added to the solution in a fume hood. The solution was allowed to cool down and then quantitatively transferred into 50-ml volumetric flasks and made the volume up to the mark with DI water. The absorbance of the solution was measured with a UV/VIS spectrophotometer (Lambda EZ 150, PerkinElmer, USA) at 410 nm. The amount of the nitrate ions adsorbed on per unit mass of adsorbent was calculated using Eq. 4 (Zulfikar et al. 2013; Ok et al. 2007):

$$q_e = \left[\frac{C_o - C_e}{m}\right] \times v \quad (4)$$

where C_o and C_e are the initial and equilibrium concentrations (in mg L^{-1}) of NO_3^-, m is the mass of material (in g), and v is the volume of solution (in L).

To predict the sorption mechanism, different kinetic models including first-order, second-order, pseudo-first-order, pseudo-second-order, Elovich, power function, and intraparticle diffusion (Eqs. 5–11, respectively) were applied (Ahmad et al. 2013b).

$$\ln q_t = \ln q_o - k_1 t \quad (5)$$

$$\frac{1}{q_t} = \frac{1}{q_o} - k_2 t \quad (6)$$

$$\ln(q_e - q_t) = \ln q_e - k_1' t \quad (7)$$

$$\frac{t}{q_t} = \frac{1}{k_2' q_e^2} + \frac{1}{q_e} t \quad (8)$$

$$q_t = \frac{1}{\beta}\ln(\alpha\beta) + \frac{1}{\beta}\ln t \quad (9)$$

$$\ln q_t = \ln b + k_f(\ln t) \quad (10)$$

$$q_t = c + k_{id} t^{0.5} \quad (11)$$

where q_t and q_o are amounts of NO_3^- adsorbed at time t and time 0 min, respectively (in mg g^{-1}), t is the time interval, k_1 and k_2 are the first- and second-order rate constants, respectively, q_e is the sorption capacity at equilibrium (in mg g^{-1}), k_1'

and k_2' are the pseudo-first- and pseudo-second-order rate constants, respectively, α is the initial sorption rate (in mg g^{-1} min^{-1}), β is the sorption constant, b is the rate constant, k_f is the rate coefficient value (in mg g^{-1} min^{-1}), k_{id} is the apparent diffusion rate constant (in [mg g^{-1}]$^{-0.5}$), and c is the diffusion constant.

The standard error of estimate (SEE) was calculated to determine the closeness between the experimental adsorption data and the model predicted data (Foo and Hameed 2010).

$$\mathrm{SEE} = \sum_{i=1}^{n} (q_{em} - q_{ec})^2 \quad (12)$$

where q_{em} and q_{ec} are measured and calculated nitrate adsorption capacities (mg g^{-1}) of the materials and n is the number of measurements.

Equilibrium sorption experiments

Multiple solute working solutions of nitrate and chloride ions were prepared using nitrate and chloride standards (Hach Company, USA). Nitrate solutions with concentrations 0, 10, 20, 50, 100, and 200 mg L^{-1} were prepared. Each nitrate solution also contained four levels of chloride ions, i.e., 0, 25, 50, and 100 mg L^{-1}. The pH was adjusted at 5 for all working solutions. Forty milliliters of the working solution was added to polypropylene conical tubes and adsorbent material was added at the rate of 1 g L^{-1}. Tubes were shaken at 150 rpm for 24 h to reach equilibrium. Solutions were then separated from the materials by centrifugation at 3500 rpm for 20 min, filtered through Whatman filter paper, and subjected to nitrate and chloride analysis. Chloride ions in the solution were measured by titration with silver nitrate (Richard 1954), while nitrate ions were determined by the procedure reported by Jagessar and Sooknundun (2011) as described earlier. Three replicates of each material and a blank were performed. The amount of nitrate sorbed (q_e in mg g^{-1}) on the materials was calculated by Eq. 4.

Various two-parameter-based equilibrium isotherm models were applied to estimate effective sorption of the prepared materials. Non-linear forms of the Freundlich and Langmuir equations (Eqs. 13 and 14, respectively) were exploited to fit the experimental sorption isotherms (Ahmad et al. 2013a).

$$q_e = K_F C_e^{1/n} \quad (13)$$

$$q_e = \frac{Q_L C_e K_L}{1 + K_L C_e} \quad (14)$$

where K_F is the Freundlich sorptive affinity parameter (L g^{-1}), $1/n$ is the Freundlich component related to linearity, Q_L is the Langmuir maximum adsorption capacity (mg g^{-1}), and K_L is the Langmuir sorption equilibrium constant (L mg^{-1}).

Results and discussion

Material characterization

Proximate and chemical analyses of the prepared materials are presented in Table 1. pH of the date palm tree leaf BM was 5.95, which was increased after pyrolysis to 10.23 in BC. The EP was alkaline with pH of 8.86 because of calcite ($CaCO_3$). Likewise, the pH of EP-BC composite was 10.03. However, pH of the nZVI-BC composite was 6.15. The increase in pH with thermal treatment might be due to higher basic functional groups, alkali salt separation from organic compounds and lower acidic functional groups (Mukherjee et al. 2011). On the other hand, lower pH of nZVI-BC could be due to several times washing of nZVI-BC composite that might have washed out the soluble basic cations. The low CEC of BC (39.86 cmol kg^{-1}) and EP-BC composite (23.28 cmol kg^{-1}) than BM (70.30 cmol kg^{-1}) could be due to loss in surface functional groups upon pyrolysis (Joseph et al. 2010), while it increased in nZVI-BC composite to 72.55 cmol kg^{-1} probably due to the presence of nano zerovalent iron. Excluding the eggshell powder contribution in yield, EP-BC composite showed 28.05% increase in yield compared to BC. An increase in ash contents from 14.01% in BM to 40.09% in BC was due to condensation and formation of mineral compounds during pyrolysis (Lehmann and Joseph 2009), while even higher ash contents in nZVI-BC and EP-BC composites (60.87 and 39.48%, respectively) were due to relatively higher resistance to thermal degradability of eggshells and iron particles. Resident matter increased from 15.52% in BM to 49.89 and 41.13% in BC and EP-BC composite, respectively, while in nZVI-BC composite, the resident matter decreased to 10.64%. This reduction in a resident matter of nZVI-BC composite might be due to the presence of graphene and Fe_3C species which remained undecomposed and confused with ash contents. Surface morphology of the materials as analyzed by SEM images is presented in Fig. 1. Pyrolysis resulted in increased porosity and channelized structure in BC due to volatilization of the organic materials (Usman et al. 2015). The nZVI-BC composite showed tube-like structures of Fe^0 on the surface of BC. Likewise, a coating of EP particles was observed on the BC matrix in EP-BC composite. X-ray diffraction spectra suggested the presence of various inorganic minerals in the materials (Fig. 2). Production of Fe^0 was confirmed by the presence of peaks at $2\theta = 44$ and 63 in the nZVI-BC composite. Fe_3O_4, Fe_3C, and graphene were also detected at 2θ = 35, 54, and 18.5, respectively in the nZVI-BC composite. A peak at $2\theta = 29.3$ was attributed to calcite ($CaCO_3$) in EP, which was further intensified in EP-BC composite due to carbonation, indicating the conversion of evolved CO_2 from biomass combustion to $CaCO_3$. Calcite was also observed at 2θ = 29.3 in BM which reduced in BC and nZVI-BC composite. A peak at $2\theta = 21.48$ represents mellite mineral in BM,

Table 1 Proximate and chemical analyses of date palm tree leaf waste biomass (BM), biochar (BC), eggshell powder (EP), BC composite with nZVI (nZVI-BC), and BC composite with EP (EP-BC)

Parameters	BM	BC	EP	nZVI-BC	EP-BC
pH	5.95	10.23	8.86	6.15	10.03
EC (dS m^{-1})	3.25	5.55	0.22	3.36	2.92
CEC (cmol kg^{-1})	70.30	39.86	6.04	72.55	23.28
Yield (%)	–	41.32	–	–	52.91
Moisture (%)	4.98	1.01	0.85	3.96	0.64
Mobile matter (%)	65.48	9.02	–	18.88	18.75
Ash (%)	14.01	40.09	–	60.87	39.48
Resident matter (%)	15.52	49.89	–	10.64	41.13

which reduced in BC and nZVI-BC. Sylvite (KCl) at $2\theta = 26.5$ and halite peaks at $2\theta = 28$ and 64.5 were prominent in BM, while it reduced in BC and diminished in the nZVI-BC composite. Sylvite (2θ = 39.5 and 49) and halite (2θ = 44) were also detected in EP and EP-BC composite. Surface area, pore volume, and pore diameter as accessed by BET analysis are shown in Table 2. The nZVI-BC composite exhibited highest surface area of 220.92 m^2 g^{-1} followed by BC (164.73 m^2 g^{-1}), EP-BC composite (114.49 m^2 g^{-1}), EP (1.41 m^2 g^{-1}), and BM (0.46 m^2 g^{-1}). Highest surface area of the nZVI-BC composite was due to the presence of Fe^0 particles on the BC matrix in the composite. FTIR spectra of the synthesized and pristine materials are shown in Fig. 3. A band at 3426 cm^{-1} in nZVI-BC composite represented stretching vibration of –OH, suggesting the formation of ferrioxyhydroxide (FeOOH) layer on Fe^0 nanoparticles (Singh et al. 2011). A broadband at 3300 cm^{-1} in BM and nZVI-BC was due to the presence of O-H stretches of H-bounding of water molecules, which was further overlapped by N-H symmetric vibrations of chitosan in nZVI-BC composite (Negrea et al. 2015). Another band at 1625 cm^{-1} in nZVI-BC composite was also designated as N-H groups due to the presence of chitosan (Negrea et al. 2015). Bands around 2900 cm^{-1} in BM were due to O-H and aliphatic C-H stretching, representing hemicellulose and cellulose (Ahmad et al., 2017a) which were lost in BC, nZVI-BC, and EP-BC due to the removal of aliphatic compounds and polar functional groups during pyrolysis. A sharp band at 860 and 1400 cm^{-1} in EP and EP-BC composite was ascribed to C-O stretches which confirmed the presence of CaO and $CaCO_3$. The sharpness of CaO and $CaCO_3$ bands increased in EP-BC composite compared to ES which indicated CO_2 absorption by EP-BC composite suggesting its potential for climate change mitigation. The TGA thermograms showed a decrease in weight loss in BC composites compared with the BM (Fig. 4). BM showed 81.14% weight loss, while BC, EP, nZVI-BC, and EP-BC showed 62.63, 48.34, 41.23, and 61.19% weight losses, respectively. Lowest weight loss in nZVI-BC composite might be due to the resistance of iron towards thermal degradability. Weight loss around temperature 200 °C in BM and BC was due to loss of non-structural free water. Curve around 300, 400, 420, and 500 °C in BM, BC, EP-BC, and nZVI-BC composite, respectively, represented weight loss due to decomposition of cellulosic and

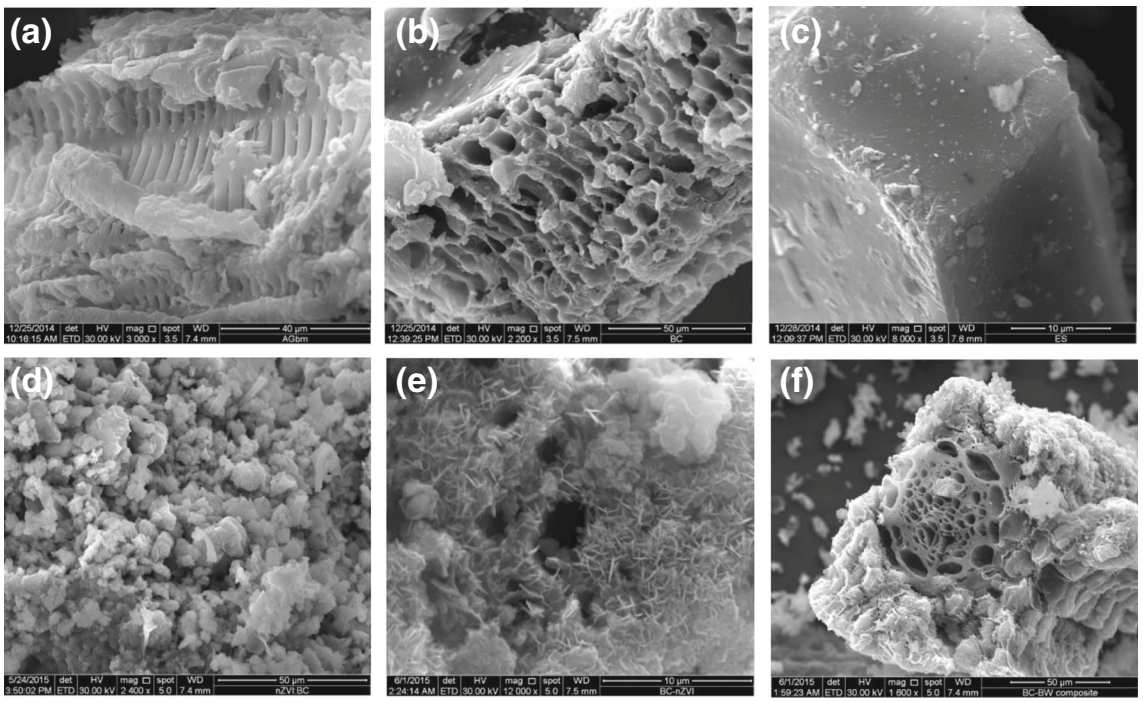

Fig. 1 Scanning electron microscope (SEM) images of **a** date palm tree leaf waste biomass (BM), **b** date palm tree leaf waste biochar (BC), **c** eggshell powder (EP), **d**. **e** nano zerovalent iron-composited BC (nZVI-BC), and **f** EP-composited BC (EP-BC)

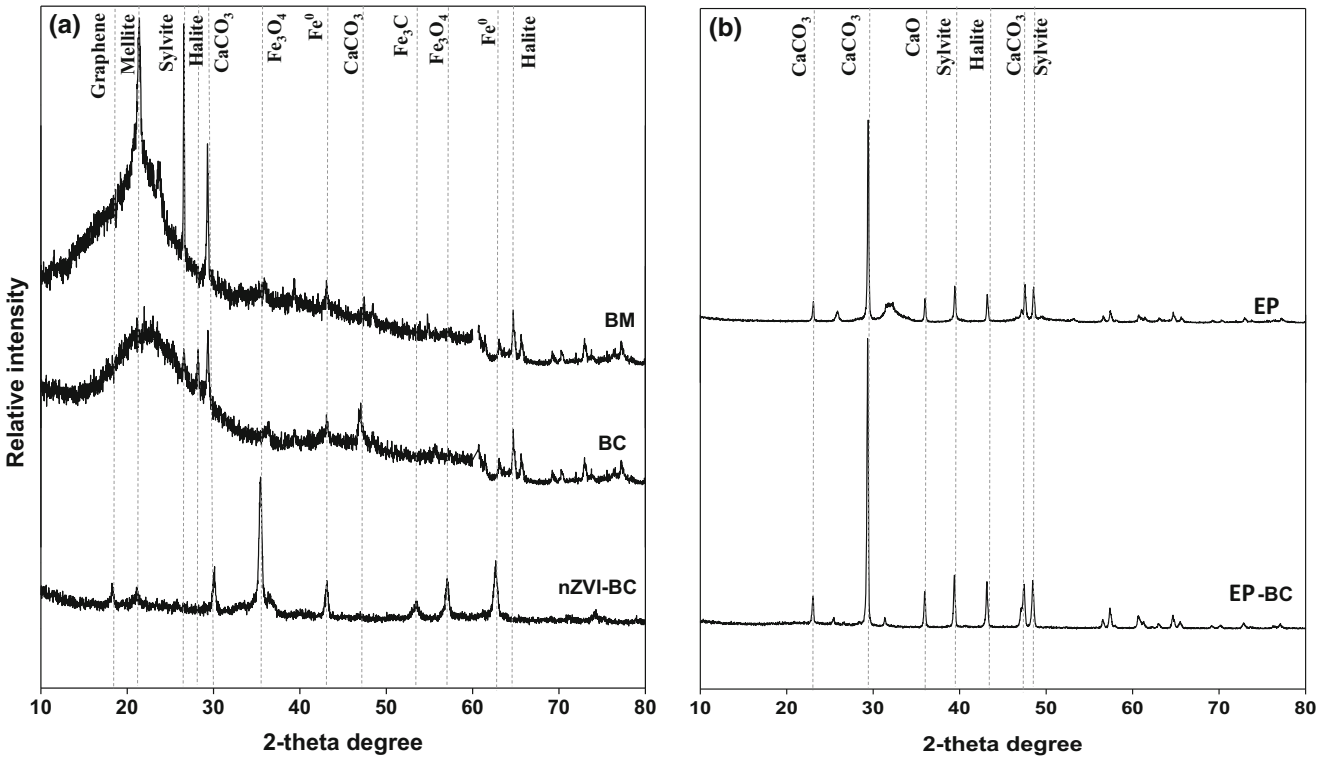

Fig. 2 XRD patterns of **a** date palm tree leaf waste biomass (BM), its derived biochar (BC), and nano zerovalent iron-composited BC (nZVI-BC) and **b** eggshell powder (EP) and its composite with BC (EP-BC)

hemicellulosic compounds (Yang et al. 2007). Complete weight loss of the materials occurred at a temperature around 630, 850, 920, 900, and 1010 °C for nZVI-BC composite, EP-BC composite, EP, BM, and BC, respectively, due to the degradation of lignin (Hernandez-Mena et al. 2014). Moreover, BC composites showed greater stability than BC and BM, which could aid in greater carbon sequestration potential of the BC composites. Elemental composition of the materials showed highest total C contents in BC (46.23%), followed by BM (44.21%), EP-BC (36.29%), and nZVI-BC (29.50%), while EP exhibited lowest C contents (16.31%) (Table 3). Increased C contents in BC composites compared to BM were due to carbonization during pyrolysis (Gai et al. 2014). Lowest O contents (4.19%) of nZVI-BC composite suggested that the composite has reductive characteristics. Interestingly, the H contents decreased in BC and EP-BC composite compared with BM due to loss of H-containing functional groups as a result of pyrolysis but increased in the nZVI-BC composite. Increased H contents in nZVI-BC composites might be due to the production of H_2 gas during reduction of Fe_2^+ by BH_4^-. The structure of EP-BC composite was designated as highly aromatic due to minimal H/C molar ratio (0.509), while of the nZVI-BC, composite was designated as minimal polar due to lowest O/C molar ratio (0.107). Overall, nZVI-BC composite contained highest H and N contents, while lowest O contents and O/C molar ratio among all synthesized materials.

Kinetic sorption

Kinetic sorption trial was conducted at a constant temperature (23 ± 02 °C) to investigate the rate of nitrate ion sorption onto synthesized materials. Dynamics of nitrate sorption are presented in Fig. 5. Plots of nitrate sorption dynamics represented three stages of sorption, i.e., rapid, relatively slow, and equilibrium. The nZVI-BC composite exhibited maximum sorption by removing 42.43% nitrate ions during first 3 h, while BC, EP-BC composite, and EP showed 12.13, 12.04, and

Table 2 Surface area, pore size, and pore volume analyses results of date palm tree leaf waste biomass (BM), biochar (BC), eggshell powder (EP), BC composite with nZVI (nZVI-BC), and BC composite with EP (EP-BC)

Sample	Surface area ($m^2\ g^{-1}$)	Pore volume ($cm^3\ g^{-1}$)	Pore diameter (nm)
BM	0.4629	0.00207	24.565
BC	164.73	0.03491	4.9185
EP	1.4050	0.00842	30.219
nZVI-BC	220.92	0.06082	5.8193
EP-BC	114.49	0.18083	8.9448

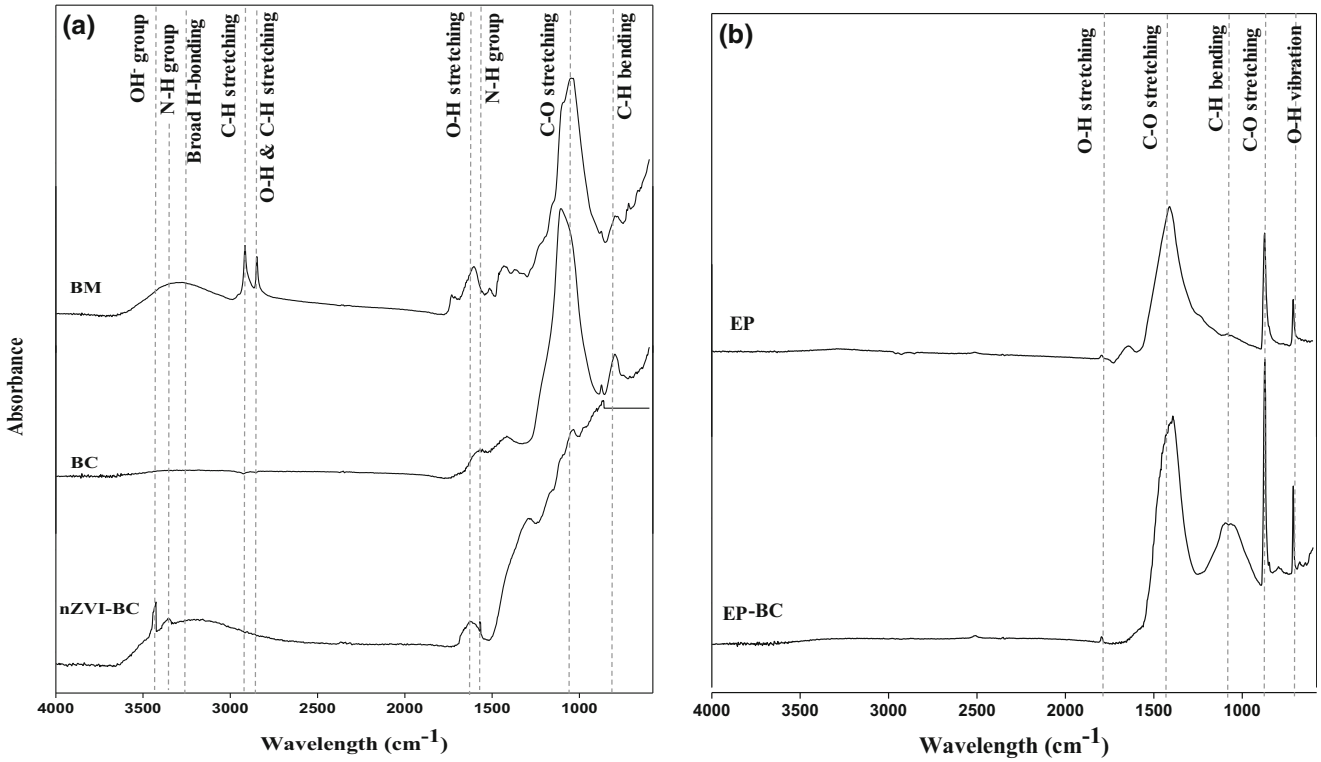

Fig. 3 FTIR spectra of **a** date palm tree leaf waste biomass (BM), its derived biochar (BC), and nano zerovalent iron-composited BC (nZVI-BC) and **b** eggshell powder (EP) and its composite with BC (EP-BC)

4.59% removal, respectively, during first 3 h. The nZVI-BC composite, EP-BC composite, BC, and EP removed 43.00, 16.06, 12.61, and 8.60% of nitrate, respectively, after 24 h. Rapid sorption stage occurred during first 3 h in BC and nZVI-BC composite and 5 h in EP-BC composite and 8 h in EP followed by slow sorption stage, which continued till equilibrium stage (24 h). Higher reaction rates of BC and nZVI-BC composite during first 3 h indicated the high availability of sorption sites, which were gradually filled up by nitrate ions in 8 h, resulting in slower sorption rate. Various kinetic models such as first-order, second-order, pseudo-first-order, pseudo-second-order, Elovich, intraparticle diffusion, and power function were applied to the sorption data. Based on R^2 and SEE values calculated from kinetic models (Table 4), it was noted that generally the fitness of the models was in the order of pseudo-second-order > power function > Elovich > intraparticle diffusion. First-order, pseudo-first-order, and second-order models were found to be inappropriate to ascribe the nitrate sorption onto the materials. Highest R^2 values of pseudo-second-order for nZVI-BC composite (0.99), EP-BC

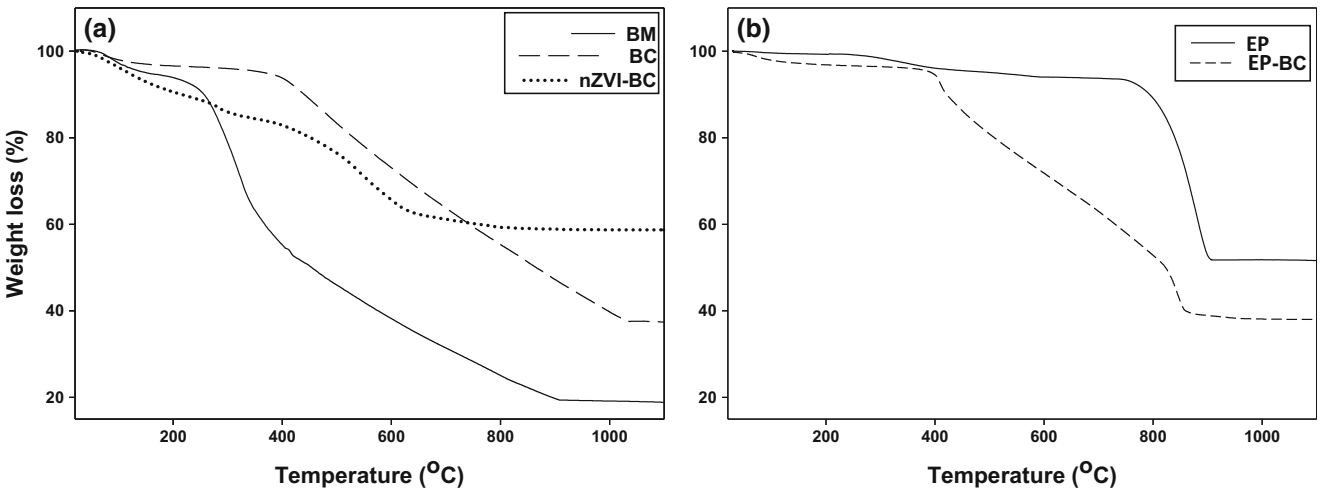

Fig. 4 Thermogravimetric analysis (TGA) of **a** date palm tree leaf waste biomass (BM), its derived biochar (BC), and nano zerovalent iron-composited BC (nZVI-BC) and **b** eggshell powder (EP) and its composite with BC (EP-BC)

Table 3 Elemental composition (%) and H/C and O/C molar ratios of date palm tree leaf waste biomass (BM), biochar (BC), eggshell powder (EP), BC composite with nZVI (nZVI-BC), and BC composite with EP (EP-BC)

Sample	N	C	H	S	O	H/C	O/C
BM	2.92	44.21	8.88	0.00	29.98	2.394	0.508
BC	0.00	46.23	2.05	0.00	11.42	0.525	0.185
EP	0.00	16.31	2.61	0.00	76.22	1.907	3.509
nZVI-BC	1.38	29.50	4.06	0.00	4.19	1.641	0.107
EP-BC	0.00	36.29	1.55	0.00	22.68	0.509	0.469

composite (0.99), BC (0.97), and EP (0.89) suggested that this model was strongly fitted for nitrate sorption onto these materials. Additionally, power function and Elovich and intraparticle diffusion models were also fitted to the experimental data of BC and its derived composites (nZVI-BC and EP-BC). SEE was found to be less than unity in all the models suggesting the minimal difference between experimental and model predicted sorption data. Parameters obtained from nitrate sorption dynamics are shown in Table 5. Higher rate constants as obtained from power function (b = 0.392) and intraparticle diffusion (k_{id} = 2.45 [mg g^{-1}]$^{-0.5}$) for nZVI-BC composite suggested it required a short time to sorb nitrate ion as compared to other materials. Followed by nZVI-BC composite, EP-BC composite showed highest rate constants as obtained from power function (b = −1.17) and intraparticle diffusion (k_{id} = 0.9688 [mg g^{-1}]$^{-0.5}$), while pseudo-second-order rate constant was maximum in EP (0.0002). Initial sorption rate of pseudo-second-order (h) was 1.680, 0.390, 0.292, and 0.205 mg g^{-1} min^{-1} and Elovich model (α) was 16.069, 5.8511, 4.523, and 3.2082 mg g^{-1} min^{-1} for nZVI-BC composite, EP-BC composite, BC, and EP, respectively. The diffusion constant for intraparticle diffusion (c) was 23.940, 4.809, 4.822, and −1.523 for nZVI-BC composite, EP-BC composite, BC, and EP, respectively, indicating highest nitrate sorption rate onto nZVI-BC composite compared to other materials. According to pseudo-second-order, power function, Elovich, and interparticle diffusion, nZVI-BC composite exhibited highest initial sorption rate. Based on sorption dynamics, it was revealed that pseudo-second-order, power function, and Elovich models well described the sorption of nitrate on the materials following sorption rate in order of nZVI-BC > EP-BC > BC > EP.

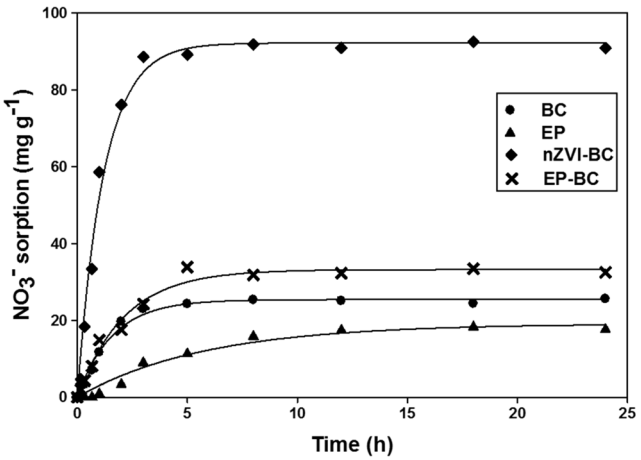

Fig. 5 Sorption kinetics of nitrate onto date palm tree leaf biochar (BC), eggshell powder (EP), nano zerovalent iron-composited BC (nZVI-BC), and EP-composited BC (EP-BC)

Equilibrium sorption

To investigate the sorption efficiency of the synthesized materials towards nitrate ions, equilibrium sorption batch experiments were conducted. Langmuir and Freundlich isotherm models were employed to reveal equilibrium amount of nitrate ions adsorbed on the sorbent at a constant temperature. Non-linear forms of the models were applied to avoid error variance. Sorption isotherms of Langmuir and Freundlich models (subpanels a and b of Fig. 6, respectively) indicated that amount of nitrate ions sorbed (Q_e) onto the sorbent material increased with an increase in initial concentrations. Ahmad et al. (2017b) and Ahmad et al. (2012) reported that concentration of initial ions decides the type of equilibrium isotherm. At low initial concentrations (up to 50 mg L^{-1}), sorption was very high developing an H-type isotherm due to strong adsorbate-adsorptive interactions indicating the presence of more sorption-active sites. At initial concentrations of above 50 mg L^{-1}, sorption was described by an L-shaped isotherm suggesting less availability of the active sites. Non-linear parameters obtained from Langmuir and Freundlich isotherms are shown in Table 6. Both models fitted well to the sorption data showing R^2 values in the range of 0.93–0.98 and 0.90–0.99, respectively. Maximum sorption capacity (Q_L) predicted by Langmuir isotherm followed the order of nZVI-BC composite (148.10 mg g^{-1}) > EP-BC composite (72.77 mg g^{-1}) > EP (26.87 mg g^{-1}) > BC (23.93 mg g^{-1}), suggesting highest sorption of nitrate ions onto nZVI-BC composite. Sorptive affinity (K_F) predicted by Freundlich isotherm followed the order of nZVI-BC composite (8.49 L g^{-1}) > EP (3.86 L g^{-1}) > BC (1.99 L g^{-1}) > EP-BC composite (1.89 L g^{-1}), suggesting highest sorption of nitrate ions onto nZVI-BC composite. Freundlich predicted $1/n$ values were in range of 0.365 to 0.622 (< 1) for all the sorbents, suggesting that sorptive affinity was favorable at lower initial ion concentration due to strong bonding between nitrate ions and sorbents and unfavorable at higher initial ion concentration due to surface loading (Site 2001; Tseng and Wu 2009).

Effect of coexisting chloride ions on nitrate sorption

Chloride ions exhibited an adverse effect on nitrate removal efficiencies from aqueous solution using synthesized

Table 4 Coefficients of determination (R^2) and standard errors of estimate (SEE) of kinetic models for nitrate sorption onto date palm leaf waste-derived biochar (BC), eggshell powder (EP), nano zerovalent iron-composited biochar (nZVI-BC), and EP-composited BC (EP-BC)

Adsorbent	First-order		Second-order		Pseudo-first-order		Pseudo-second-order		Elovich		Intraparticle diffusion		Power function	
	R^2	SEE	R^2	SEE	R^2	SEE	R^2	SEE	R^2	SEE	R^2	SEE	R^2	SEE
BC	0.48	0.002	0.100	0.110	0.560	0.000	0.970	0.048	0.870	0.000	0.720	1.500	0.850	0.000
EP	0.76	0.006	0.200	0.044	0.910	0.000	0.890	0.037	0.760	0.000	0.900	0.480	0.770	0.910
nZVI-BC	0.42	0.030	0.090	0.002	0.670	0.000	0.990	0.054	0.880	0.008	0.660	0.003	0.900	0.690
EP-BC	0.56	0.060	0.150	0.015	0.760	0.059	0.990	0.028	0.880	0.000	0.790	0.002	0.950	0.420

materials (Fig. 7). Generally, highest nitrate sorption was observed in the absence of chloride ions (0 mg L^{-1}), and then a gradual decrease in nitrate sorption occurred with increasing the chloride ion concentration up to 100 mg L^{-1} with all the materials. Non-linear parameters of Langmuir and Freundlich's isotherm representing the effect of chloride ions on the sorption of nitrate ions are shown in Tables S1 and S2, respectively. The maximum decrease in nitrate sorption capacity was observed with nZVI-BC composite (103.13%), followed by EP-BC composite (52.35%), EP (30.13%), and BC (8.50%) as predicted by Langmuir model at 100 mg L^{-1} chloride coexistence. Decrease in nitrate sorption with increasing chloride concentration might be due to more free active sites available for nitrate at low chloride concentration, but as the chloride ion concentration increased in the solution, it started occupying the free active sites on the adsorbent surface as a result of competitive effect (Hu et al. 2015). The adverse effect of other anions on nitrate sorption has already been reported. For example, Bhatnagara and Sillanpaa (2011) and Khan et al. (2011) reported that presence of coexisting anions reduced nitrate sorption due to competition for active sites in order of carbonate > phosphate > chloride > sulfate. According to Islam et al. (2010), adverse effect of other coexisting anions on nitrate sorption was in the order of chloride > carbonate > sulfate > phosphate. Interestingly, nZVI-BC composite performed well by removing more nitrate from aqueous solutions compared to other materials even in the presence of higher chloride ion concentration (100 mg L^{-1}). At higher coexisting chloride ions, nZVI-BC composite showed maximum nitrate sorption of 30.80 mg g^{-1}, which is 26.82, 46.41, and 56.80% higher compared to EP-BC composite, BC, and EP, respectively. Nabizadeh et al. (2014) reported that functionalized polyacrylonitrile-coated with iron oxide nanoparticles (PAN-Oxime-Fe_2O_3) has maximum sorption capacity of 16.17 mg g^{-1} for nitrate ions in aqueous solution. In the presence of chloride ions, the removal efficiency of PAN-Oxime-Fe_2O_3 reduced by 85%. Dehghani et al. (2015) found that removal efficiency of granular ferric hydroxide for nitrate was 56.6%, which reduced to 15.8% in presence of 400 mg L^{-1} of chloride ions. These results suggest the highest potential of nZVI-BC composite for the removal of nitrate ion from contaminated real wastewater which contains various other anions as competitors for the binding sites. Therefore, nZVI-BC composite has higher removal efficiency for nitrate ions even in the presence of other competitive anions such as chlorides in the aqueous media. The nZVI-BC composite hence can be used in wastewater treatment plants for efficient removal of pollutants from the contaminated water.

Nitrate removal mechanism

To investigate the operating mechanism for nitrate removal using the synthesized materials, various kinetic and empirical models were applied to the sorption data. Different mechanisms could be involved in determining the nitrate sorption onto different materials used in this study. Based on the experimental and modeling data, best fitted Langmuir isotherm suggested monolayer sorption of nitrate ions onto materials, which was additionally aided by multi-layer sorption in nZVI-BC composite, EP and EP-BC composite as ascribed with the

Table 5 Parameters obtained from kinetic models for nitrate sorption onto date palm leaf waste-derived biochar (BC), eggshell powder (EP), nano zerovalent iron-composited BC (nZVI-BC), and EP-composited BC (EP-BC)

Adsorbent	First-order	Second-order	Pseudo-first-order		Pseudo-second-order			Elovich		Intraparticle diffusion		Power function	
	k_1	k_2	k_1'	q_e	k_2'	q_e	h	α	β	k_{id}	C	k_f	b
BC	0.0152	−0.0002	−0.0025	2.2688	4×10^{-4}	27.470	0.292	4.5423	−5.3002	0.7209	4.822	0.544	−0.223
EP	0.0145	−0.0001	−0.0034	2.8388	6×10^{-4}	18.760	0.205	3.2082	−7.1238	0.6107	−1.523	−0.549	−1.120
nZVI-BC	0.0503	0.0000	−0.0036	3.3660	2×10^{-4}	9.710	1.680	16.0690	−13.4440	2.4468	23.940	0.733	0.392
EP-BC	0.0211	−0.0001	−0.0034	2.2851	4×10^{-4}	35.590	0.390	5.8511	−7.6168	0.9688	4.809	0.607	−0.171

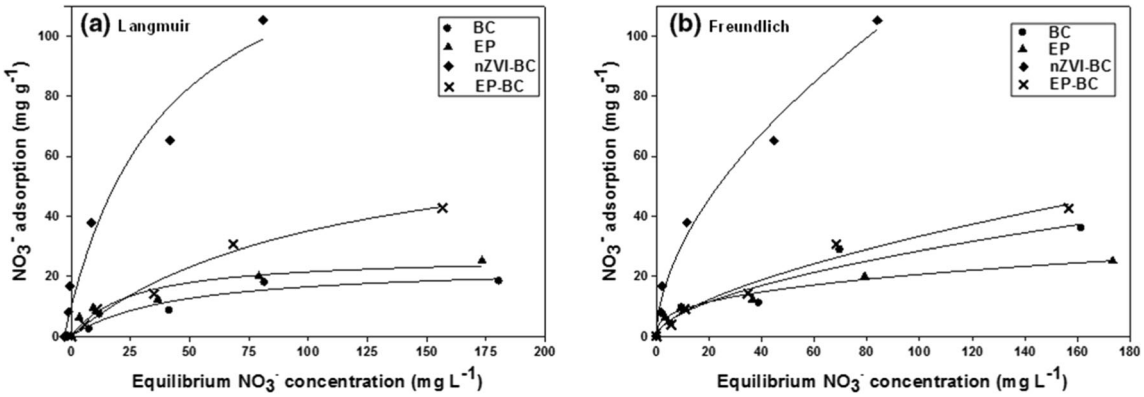

Fig. 6 Nitrate sorption isotherms fitting on **a** Langmuir and **b** Freundlich models by date palm tree leaf biochar (BC), eggshell powder (EP), nano zerovalent iron-composited BC (nZVI-BC), and EP-composited BC (EP-BC)

fitness of Freundlich isotherm indicating the presence of heterogeneous active sites. The closeness of the experimental data to the pseudo-second-order model suggested chemisorption (covalent binding with the functional groups) as a rate-limiting step for nitrate sorption onto the materials. Chemisorption was further supported by power function and Elovich models (Alberti et al. 2007). Electrostatic interaction (outer-sphere complexation) and ionic exchange could be the possible pathways for nitrate sorption onto BC composites (Chintala et al. 2013). Coexistence of chloride ions negatively affected the nitrate sorption onto different materials, which could be attributed to a competitive effect in which chloride ions quickly adsorbed on the surfaces of the sorbents resulting in increased electrostatic repulsion forces between nitrate ions and sorbent (Hu et al. 2015). As chloride ion concentration increased in aqueous solution, electrostatic repulsion got stronger resulting in reduced nitrate sorption onto the materials at higher chloride ion concentrations.

The nZVI-BC composite outperformed the other materials in removing nitrate ions from aqueous solution. The higher removal rate and capacity of nZVI-BC composite as predicted by Langmuir and Freundlich isotherms, and sorption dynamic models, could possibly be due to a combination of two processes, i.e., chemisorption and nitrate reduction. As nitrate ions come across the surface of the nZVI-BC composite, some ions are chemisorbed and other adsorbed on the surface of the matrix. The absorbed nitrate ions on the surface are further reduced by Fe^0 particles, causing high removal during initial 3 h. Nitrate reduction was further aided by intraparticle diffusion, where BC matrix facilitated mass transfer of nitrate ions onto Fe^0 particles. Due to higher surface area of the nZVI-BC composite, more nitrate ions come in contact with Fe^0 particles on the surface of the biochar matrix, resulting in increased electron transfer from Fe^0 to nitrate (Huang and Zhang 2002). In aqueous media, at pH < 7, nitrate ions are reduced by Fe^0 particles into ammonia or N_2 gas, and Fe^0 is oxidized to ferrous ion (Fe^{2+}) (Yang and Lee 2005). Post-sorption FTIR analysis was used to validate the occurrence of chemisorption and redox reactions (Fig. 8). The presence of two new absorption bands at 2341 and 1790 cm^{-1} in nZVI-BC composite represented N-H group, which could be an indication for the production of a new chemical species ferric nitrate ($Fe(NO_3)_3{\cdot}9H_2O$) as a result of chemisorption. An absorption band appeared at 681 cm^{-1} indicated the presence of iron oxide (FeO), which has formed as a result of Fe^0 oxidation. Conversion of Fe^0 to iron oxide is confirmed by a redox reaction, in which Fe^0 is oxidized to FeO and NO_3^- is reduced to NH_3 or N_2 gas. Possible pathways for reduction of nitrate to nitrogen or ammonia are as follows (Yang and Lee 2005; Choe et al. 2000; Li et al. 2010):

$$5Fe^0 + 2NO_3^- + 12H^+ \leftrightarrow 5Fe^{2+} + N_2 + 6H_2O \quad (15)$$

$$4Fe^0 + NO_3^- + 10H^+ \leftrightarrow 4Fe^{2+} + NH_4^+ + 3H_2O \quad (16)$$

After the oxidation of iron, reduction of nitrate ion by Fe^0 is further facilitated by iron oxide/magnetite as shown in Eq. 17.

$$NO_3^- + 2.82Fe^0 + 0.75Fe^{2+} + 2.25H_2O \leftrightarrow NH_4^+ + 1.19Fe_3O_4 + 0.5OH^- \quad (17)$$

Solution pH increased from initial pH (5) to final pH in the range of 6–7.65 in kinetic sorption, while in the

Table 6 Non-linear parameters of Langmuir and Freundlich isotherms indicating nitrate sorption onto date palm leaf waste-derived biochar (BC), eggshell powder (EP), nano zerovalent iron-composited BC (nZVI-BC), and EP-composited BC (EP-BC)

Sorbents	Langmuir isotherm			Freundlich isotherm		
	Q_L (mg g^{-1})	K_L (L g^{-1})	R^2	K_F (L g^{-1})	1/n	R^2
BC	23.93	0.022	0.93	1.99	0.445	0.90
EP	26.87	0.040	0.93	3.86	0.365	0.99
nZVI-BC	148.10	0.024	0.96	8.49	0.562	0.99
EP-BC	72.77	0.009	0.98	1.89	0.622	0.98

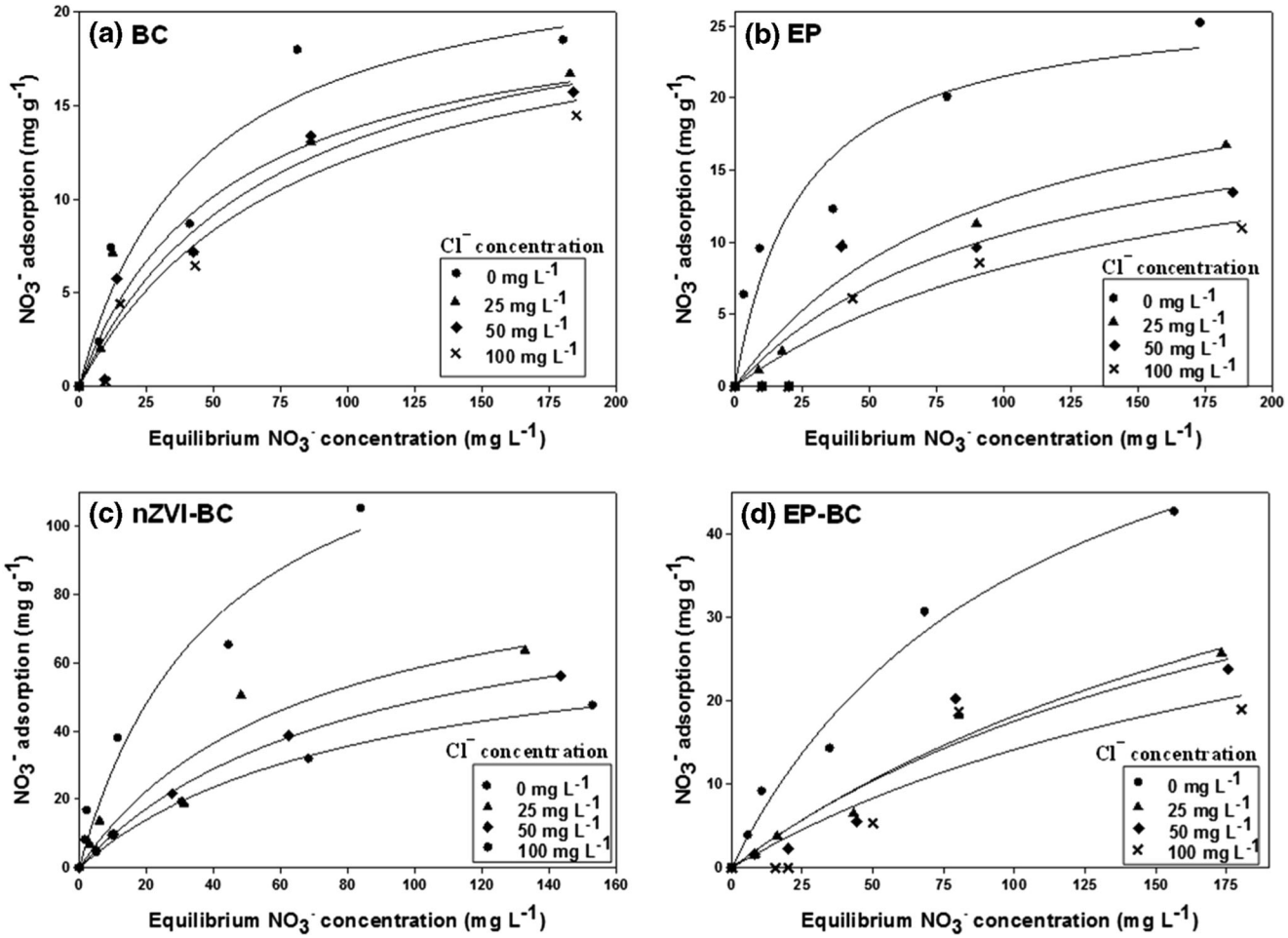

Fig. 7 Nitrate sorption onto **a** date palm tree leaf biochar (BC), **b** eggshell powder (EP), **c** nano zerovalent iron-composited BC (nZVI-BC), and **d** EP-composited BC (EP-BC) as influenced by the presence of various chloride ion concentrations in the aqueous media (0, 25, 50, and 100 mg Cl^{-} L^{-1})

range of 6.21–7.51 in equilibrium sorption batch suggesting that pH was remained near neutral during the sorption batches (Fig. S2). No significant changes in nitrate sorption were observed due to pH variations (as pH was near neutral). Hu et al. (2015) reported that a pH range of 3 to 10 has no effects on nitrate removal efficiency. Furthermore, Huang and Zhang (2002) reported the formation of iron oxide and magnetite in $Fe^0/NO_3^-/H_2O$ system in the pH range of 5–8, which is in agreement with this study.

Followed by the nZVI-BC composite, higher sorption rate and capacity of EP-BC composite were due to combined effect of eggshell powder and biochar. Calcium-based sorbents have very lower affinity for nitrate because there are less chances for nitrate to complex with cation (Park et al. 2008), but if composited with biochar, nitrate may bind with calcium to form calcium nitrate due to chemisorption of nitrate ions onto EP-BC surfaces, and biochar matrix may facilitate this binding. Covalent binding of nitrate ions with –OH functional groups in EP-BC composite was the operating mechanism for nitrate sorption as indicated in FTIR spectra (Fig. 8) with the formation N-H group (Islam et al. 2010).

Conclusion

Nano zerovalent iron-composited biochar and waste hen eggshell powder-composited biochar were synthesized by using date palm leaf waste biochar and tested for nitrate removal from aqueous media. Effect of coexisting chloride ions was also investigated on nitrate sorption. Graphene and nano zerovalent iron (Fe^0) synthesis on biochar matrix was confirmed by XRD analysis. The nZVI-BC composite showed highest sorption capacity towards nitrate removal from aqueous solution. The highest nitrate removal capacity of the nZVI-BC composite was related to a combination of two processes: (1) chemisorption of nitrate ions on the surface of composite resulting in the formation of new N-containing species such as ferric nitrate ($Fe(NO_3)_3 \cdot 9H_2O$) and (2) reduction of nitrate ions by Fe^0 to ammonia or

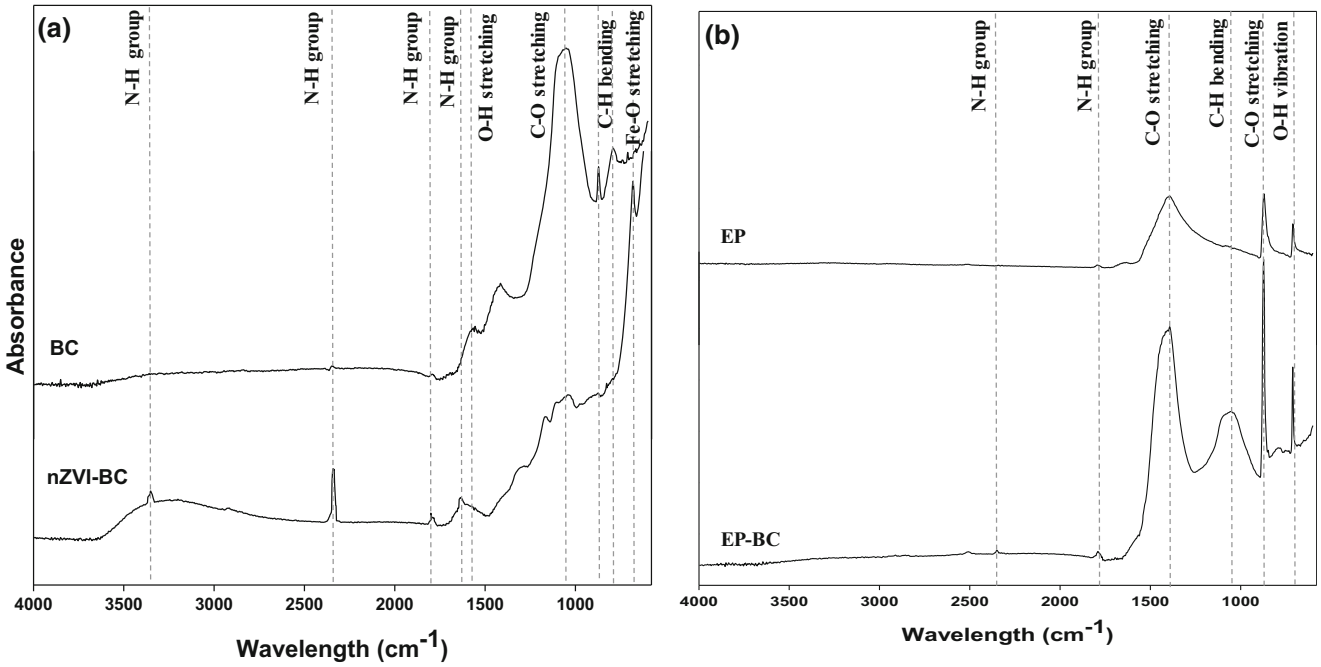

Fig. 8 Post-sorption FTIR analyses of date palm tree leaf biochar (BC), eggshell powder (EP), nano zerovalent iron-composited BC (nZVI-BC), and EP-composited BC (EP-BC)

nitrogen gas. Following nZVI-BC composite, higher nitrate removal of EP-BC composite was attributed to the combined action of eggshell and biochar. Calcium-based sorbents have very lower affinity for nitrate because there are less chances for nitrate to complex with cation, but if composited with biochar, nitrate may bind with calcium to form calcium nitrate due to chemisorption of nitrate ions onto EP-BC surfaces. The adverse effect of chloride ions on nitrate removal was because of competition for active sorption sites. Nitrate sorption was decreased with increasing chloride ion concentration in the solution. Synthesized nZVI-BC and EP-BC composites could efficiently be applied to remove nitrate ion from water streams and to retain nitrate ion in soils in order to prevent leaching and seepage to underground or nearby water bodies. As for date palm tree waste and hen eggshells, waste is creating surface pollution; therefore, recycling of these waste material can not only reduce the surface pollution but can also serve as eco-friendly and cost-effective green technology to remediate various soil and water contaminants.

Acknowledgements The authors extend their appreciation to the Deanship of Scientific Research, King Saud University for funding this work through the international research group project IRG-14-02.

Compliance with ethical standards

Conflict of interest The authors declare that they have no conflict of interest.

References

Agency for Toxic Substances and Disease Registry (ATSDR) (2013) Centers for Disease Control and Prevention nitrate/nitrite toxicity. What are the US standards for nitrate and nitrite levels?, pp 1–135. http://www.atsdr.cdc.gov/csem/csem.asp?csem=28

Ahmad M, Usman RA, Lee SS, Kim S, Joo J, Yang JE, Ok YS (2012) Eggshell and coral wastes as low cost sorbents for the removal of Pb^{2+}, Cd^{2+} and Cu^{2+} from aqueous solutions. J Indust Eng Chem 18: 198–204

Ahmad M, Lee SS, Oh SE, Mohan D, Moon DH, Lee YH, Ok YS (2013a) Modeling adsorption kinetics of trichloroethylene onto biochars derived from soybean stover and peanut shell wastes. Environ Sci Pollut Res 20:8364–8373

Ahmad M, Lee SS, Rajapaksha AU, Vithanage M, Zhang M, Cho JS, Lee SE, Ok YS (2013b) Trichloroethylene adsorption by pine needle biochars produced at various pyrolysis temperatures. Bioresour Technol 143:615–622

Ahmad M, Ahmad M, Usman AR, Al-Faraj AS, Abduljabbar A, Ok YS, Al-Wabel MI (2017a) Date palm waste-derived biochar composites with silica and zeolite: synthesis, characterization and implication for carbon stability and recalcitrant potential. Environ Geochem health 1–18. https://doi.org/10.1007/s10653-017-9947-0

Ahmad M, Ahmad M, Usman AR, Al-Faraj AS, Ok YS, Hussain Q, Abduljabbar A, Al-Wabel MI (2017b) An efficient phosphorus scavenging from aqueous solution using magnesiothermally modified bio-calcite. Environ Technol 1-12. https://doi.org/10.1080/09593330.2017.1335349

Alberti G, Amendola V, Pesavento M, Biesuz R (2007) Beyond the synthesis of novel solid phases: review on modeling of sorption phenomena. Coordin Chem Rev 256:28–45

American Society for Testing and Materials (ASTM) (1989) Annual book of ASTM standards D1762-84 281–282. Philadelphia, PA, USA

Beck DA, Johnson GR, Spolek GA (2011) Amending green roof soil with biochar to affect runoff water quantity and quality. Environ Pollut 159:2111–2118

Beesley L, Moreno-Jimenez E, Gomez-Eyles JL (2010) Effects of biochar and green waste compost amendments on mobility, bioavailability, and toxicity of inorganic and organic contaminants in a multi-element polluted soil. Environ Pollut 158:2282–2287

Bhatnagar A, Sillanpaa M (2011) A review of emerging adsorbents for nitrate removal from water. Chem Eng J 168:493–504

Blair GJ, Lefroy RDB, Lisle L (1995) Soil carbon fractions based on their degree of oxidation, and the development of a carbon management index for agricultural systems. Aust J Agric Res 46:1459–1466

Buasri A, Chaiyut N, Loryuenyong V, Wongweang C, Khamsrisuk S (2013) Application of eggshell wastes as a heterogeneous catalyst for biodiesel production. Sust Energ 1:7–13

Chang C, Lian F, Zhu L (2011) Simultaneous adsorption and degradation of g-HCH by nZVI/Cu bimetallic nanoparticles with activated carbon support. Environ Pollut 159:2507–2514

Chatterjee S, Lim SR, Woo SH (2010) Removal of reactive black 5 by zero-valent iron modified with various surfactants. Chem Eng J 160: 27–32

Chintala R, Mollinedo J, Schumacher TE, Papiernik SK, Malo DD, Clay DE, Kumar S, Gulbrandson DW (2013) Nitrate sorption and desorption in biochars from fast pyrolysis. Micropor Mesopor Mater 179: 250–257

Choe S, Chang Y, Hwang K, Khim J (2000) Kinetics of reductive denitrification by nanoscale zero-valent iron. Chemosphere 41:1307–1311

Dehghani M, Haidari E, Shahsavani S, Shamsedini N (2015) Removal of nitrate in the aqueous phase using granular ferric hydroxide. Jundishapur J Health Sci 7(2):e26419

Devi P, Saroha AK (2014) Synthesis of the magnetic biochar composites for use as an adsorbent for the removal of pentachlorophenol from the effluent. Bioresour Technol 169:525–531

Dobermann A, Cassman KG (2005) Cereal area and nitrogen use efficiency are drivers of future nitrogen fertilizer consumption. Sci. China. Ser. C Life Sciences/Chinese Acad Sci 48:745–758

Flechard CR, Nemitz E, Smith RI, Fowler D, Vermeulen AT, Bleeker A, Erisman JW, Simpson D, Zhang L, Tang YS, Sutton MA (2011) Dry deposition of reactive nitrogen to European ecosystems: a comparison of inferential models across the NitroEurope network. Atmos Chem Phys 11(6):2703–2728

Foo KY, Hameed BH (2010) Insights into the modeling of adsorption isotherm systems. Chem Eng J 156:2–10

Gai X, Wang H, Liu J, Zhai L, Liu S (2014) Effects of feedstock and pyrolysis temperature on biochar adsorption of ammonium and nitrate. PLoS One 9(12):e113888. https://doi.org/10.1371/journal.pone.0113888

Gupta AK, Gupta M (2005) Biomaterials 26:3995

Guru PS, Dash S (2014) Sorption on eggshell waste—a review on ultrastructure, biomineralization and other applications. Adv Colloid Interf Sci 209:49–67

Hernández-Mena L, Pecora A, Beraldo A (2014) Slow pyrolysis of bamboo biomass: analysis of biochar properties. Chem Eng Transac 37: 115–120. https://doi.org/10.3303/CET1437020

Hu Q, Chen N, Feng C, Hu W (2015) Nitrate adsorption from aqueous solution using granular chitosan-Fe3+complex. Appl Surface Sci 347:1–9

Huang YH, Zhang TC (2002) Kinetics of nitrate reduction by iron at near neutral pH. J Environ Eng 128:604–611

Islam M, Mishra PC, Patel R (2010) Physicochemical characterization of hydroxyapatite and its application towards removal of nitrate from water. J Environ Manag 91:1883–1891

Jagessar RC, Sooknundun L (2011) Determination of nitrate anion in waste water from nine selected areas of coastal Guyana via a spectrophotometric method. Int J Res Rev Appl Sci 7(2):203–212

Joseph SD, Camps-Arbestain M, Lin Y, Munroe P, Chia CH, Hook J, Zwieten L, Kimber S, Cowie A, Singh BP, Lehmann J, Foid N, Smernik JR, Amonette LE (2010) An investigation into the reactions of biochar in soil. Aust J Soil Res 48:501–515

Khan AM, Ahn Y, Kumar M, Lee W, Min B, Kim G, Cho D, Park WB, Jeon B (2011) Adsorption studies for the removal of nitrate using modified lignite granular activated carbon. Sep Sci Technol 46: 2575–2584

Kim DK, Zhang Y, Voit W, Rao KV, Muhammed M (2001) Synthesis and characterization of surfactant-coated superparamagnetic monodispersed iron oxide nanoparticles. J Magn Magn Mater 225: 30–36

Landon MK, Delin GN, Komor SC, Regan CP (2000) Relation of pathways and transit times of recharge water to nitrate concentrations using stable isotope. Ground Water 38:381–395

Lehmann J, Joseph S (2009) Biochar for environmental management: an introduction. In: Lehmann J, Joseph S (eds) Biochar for environmental management science and technology. Earthscan, UK, pp 1–12

Li J, Li Y, Meng Q (2010) Removal of nitrate by zero-valent iron and pillared bentonite. J Hazard Mate 174:188–193

Loganathan P, Vigneswaran S, Kandasamy J (2013) Enhanced removal of nitrate from water using surface modification of adsorbents—a review. J Environ Manag 131:363–374

Meng Y, Guan B, Wu Z, Wang D (2006) Enhanced degradation of carbon tetrachloride by surfactant-modified zero-valent iron. J Zhejiang Univ Sci 7:702–707

Mukherjee A, Zimmerman AR, Harris W (2011) Surface chemistry variations among a series of laboratory-produced biochars. Geoderma 163:247–255

Nabizadeh R, Jahangiri-rad M, Rafiee M (2014) Counterion effects on nitrate adsorption from aqueous solution onto functionalized polyacrylonitrile coated with iron oxide nanoparticles. Res J Environ Sci 8:287–293

Negrea P, Caunii A, Sarac I, Butnariu M (2015) The study of infrared spectrum of chitin and chitosan extract as potential sources of biomass. Dig J Nanomater Biostruct 10:1129–1138

Ok YS, Yang JE, Zhang YS, Kim SJ, Chung DY (2007) Heavy metal adsorption by a formulated zeolite-Portland cement mixture. J Hazard Mater 147(1):91–96

Oliveira DA, Benelli P, Amante ER (2013) A literature review on adding value to solid residues: egg shells. J Cleaner Product 46:42–47

Park JY, Byun HJ, Choi WH, Kang WH (2008) Cement paste column for simultaneous removal of fluoride, phosphate, and nitrate in acidic wastewater. Chemosphere 70:1429–1437

Phenrat T, Saleh N, Sirk K, Tilton RD, Lowry GV (2006) Aggregation and sedimentation of aqueous nanoscale zerovalent iron dispersions. Environ Sci Technol 41:284–290

Raihana MF, Sopyan I, Hamdi M, Ramesh S (2008) Novel chemical conversion of eggshell to hydroxyapatite powder. IFMBE Proc 21: 333–336

Richard LA (1954) Diagnoses and improvement of saline and alkali soils. Agriculture handbook, 60: USDA, USA

Richardson K (1997) Harmful or exceptional phytoplankton blooms in the marine ecosystem. Adv Mar Biol 31:301–385

Singh R, Misra V, Singh RP (2011) Synthesis, characterization and role of zero-valent iron nanoparticle in removal of hexavalent chromium from chromium-spiked soil. J Nanopart Res 13:4063–4073

Site AD (2001) Factors affecting sorption of organic compounds in natural sorbent/water system and sorption coefficients for selected pollutants. A review J Phys Chem Ref Data 30:187–439

Sun YP, Li XQ, Cao J, Zhang WX, Wang HP (2006) Characterization of zero-valent iron nanoparticles. Adv Colloid Interface Sci 120:47–56

Tseng R, Wu F (2009) Analyzing a liquid–solid phase countercurrent two- and three-stage adsorption process with the Freundlich equation. J Hazard Mater 162:237–248

Usman ARA, Abduljabbar A, Vithanage M, Ok YS, Ahmad M, Ahmad M, Elfaki J, Abdulazeem SS, Al-Wabel MI (2015) Biochar

production from date palm waste: charring temperature induced changes in composition and surface chemistry. J Anal Appl Pyrol 115:392–400

Uzum C, Shahwan T, Eroglu AE, Lieberwirth I, Scott TB, Hallam KR (2008) Application of zero valent iron nanoparticles for the removal of aqueous CO^{2+} ions under various experimental conditions. Chem Eng J 144:213–220

Wardle DA, Nilsson MC, Zackrisson O (2008) Fire-derived charcoal causes loss of forest humus. Science 320:629

Weyer PJ, Cerhan JR, Kross BC, Hallberg GR, Kantamneni J, Breuer G, Jones MP, Zheng W, Lynch CF (2001) Municipal drinking water nitrate level and cancer risk in older women: the Iowa women's health study. Epidemiology 12:327–338

World Health Organization, Geneva (WHO G) (2011) Guidelines for drinking-water quality, Fourth Ed. World Health Organization 216: 303–4

Wu X, Yang Q, Xu D, Zhong Y, Luo K, Li X, Chen H, Zeng G (2013) Simultaneous adsorption/reduction of bromate by nanoscale zerovalent iron supported on modified activated carbon. Ind Eng Chem Re 52:12574–12581

Xu J, Gao N, Tang Y, Deng Y, Sui M (2010) Perchlorate removal using granular activated carbon supported iron compounds: synthesis, characterization and reactivity. J Environ Sci 22:1807–1813

Xue D, Pang F, Meng F, Wang Z, Wu W (2015) Decision-tree-model identification of nitrate pollution activities in groundwater: a combination of a dual isotope approach and chemical ions. J Con Hydrol 180:25–33

Yan J, Han L, Gao W, Xue S, Chen M (2015) Biochar supported nano-scale zerovalent iron composite used as persulfate activator for removing trichloroethylene. Bioresour Technol 175:269–274

Yang GCC, Lee H (2005) Chemical reduction of nitrate by nanosized iron: kinetics and pathways. Water Res 39:884–894

Yang H, Yan R, Chen H, Lee DH, Zheng C (2007) Characteristics of hemicellulose, cellulose and lignin pyrolysis. Fuel 86:1781–1788

Ying L, Hofseth LJ (2007) An emerging role for endothelial nitric oxide synthase in chronic inflammation and cancer. Cancer Res 67(4): 1407–1410

Yuvakkumar R, Elango V, Rajendran V, Kannan N (2011) Preparation and characterization of zero valent iron nanoparticles. J Nanomater Biostruct 6:1771–1776

Zhao X, Shi Y, Cai Y, Mou S (2008) Cetyltrimethylammonium bromide-coated magnetic nanoparticles for the preconcentration of phenolic compounds from environmental water samples. Environ Sci Technol 42:1201–1206

Zhou Y, Gao G, Zimmerman AR, Chen H, Zhang M, Cao X (2014) Biochar-supported zerovalent iron for removal of various contaminants from aqueous solutions. Bioresour Technol 152:538–542

Zulfikar MA, Novita E, Hertadi R, Djajanti SD (2013) Removal of humic acid from peat water using untreated powdered eggshell as a low cost adsorbent. Int J Environ Sci Technol 10:1357–1366